Biomass-Derived Sponge-like Carbonaceous Hydrogels and Aerogels for Supercapacitors

Xi-Lin Wu,[†,‡] Tao Wen,[‡] Hong-Li Guo,[†] Shubin Yang,[‡] Xiangke Wang,[‡,*] and An-Wu Xu[†,*]

[†]School of Nuclear Science and Technology, Division of Nanomaterials & Chemistry, University of Science and Technology of China, Hefei, Anhui 230026, People's Republic of China and [‡]Key Laboratory of Novel Thin Film Solar Cells, Institute of Plasma Physics, Chinese Academy of Sciences, Hefei, Anhui, 230031, People's Republic of China

ABSTRACT As a newly developed material, carbon gels have been receiving considerable attention due to their multifunctional properties. Herein, we present a facile, green, and template-free route toward sponge-like carbonaceous hydrogels and aerogels by using crude biomass, watermelon as the carbon source. The obtained three-dimensional (3D) flexible carbonaceous gels are made of both carbonaceous nanofibers and nanospheres. The porous carbonaceous gels (CGs) are highly chemically active and show excellent mechanical flexibility which enable them to be a good scaffold for the synthesis of 3D composite materials. We synthesized the carbonaceous gel-based composite materials by incorporating Fe_3O_4 nanoparticles into the networks of the carbonaceous gels. The Fe_3O_4/CGs composites further transform into magnetite carbon aerogels (MCAs) by calcination. The MCAs keep the porous structure of the original CGs, which allows the sustained and stable transport of both electrolyte ions and electrons to the electrode surface, leading to excellent electrochemical performance. The MCAs exhibit an excellent capacitance of 333.1 $F \cdot g^{-1}$ at a current density of 1 $A \cdot g^{-1}$ within a potential window of −1.0 to 0 V in 6 M KOH solution. Meanwhile, the MCAs also show outstanding cycling stability with 96% of the capacitance retention after 1000 cycles of charge/discharge. These findings open up the use of low-cost elastic carbon gels for the synthesis of other 3D composite materials and show the possibility for the application in energy storage.

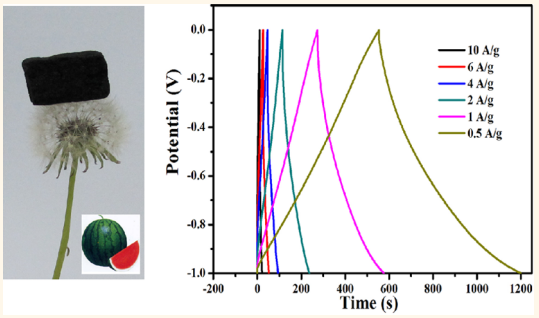

KEYWORDS: carbon materials · hydrogel · aerogel · mechanical properties · supercapacitors

Hydrogels and aerogels are two types of gels consisting of three-dimensional (3D) nanostructural solid networks with different infilling mediums in the interspaces, that is, water and air.[1] The open 3D networks with continuous nanopores in the gels can provide efficient diffusion/mass transfer of liquid/gas phase analytes or substrates.[1,2] Because of the unique properties, such as good osmotic property, high water absorptivity, and good elasticity, hydrogels are expected to have excellent performance as adsorbents,[3] materials for biomedical applications,[4] sensors,[5] catalyst supports,[6] electrode materials for batteries, and supercapacitors.[7,8] The properties of high surface area, high porosity, and low density in aerogels could lead to promising applications in many fields such as electrodes and catalysts.[9] Hydrogels can be transformed to aerogels by replacing the liquid solvent in the hydrogels or other wet gels by air without collapsing the 3D network structure.[1] Conventional methods for preparing aerogels often involve template (hard template or soft template), expensive chemicals, and supercritical drying.[1,10,11] Moreover, the prepared aerogels are also associated with the problems of poor mechanical stability. Thus, developing an environmental friendliness and low-cost approach to robust aerogels is still challenging.

Many efforts have been made aiming to synthesize new types of carbonaceous gels with multiple applications and, more importantly, to develop novel synthetic methods. Recently, carbonaceous gels based on cellulose fibers,[12,13] carbon nanotubes,[14,15] and graphene[16,17] have been successfully fabricated by different methods, including freezing−thawing,[12] hard template,[13] soft template,[14,15] hydrothermal treatment,[16] and freeze-drying.[17] Among these methods, hydrothermal treatment is considered as a

* Address correspondence to anwuxu@ustc.edu.cn, xkwang@ipp.ac.cn.

Received for review February 2, 2013 and accepted March 26, 2013.

Published online April 02, 2013
10.1021/nn400566d

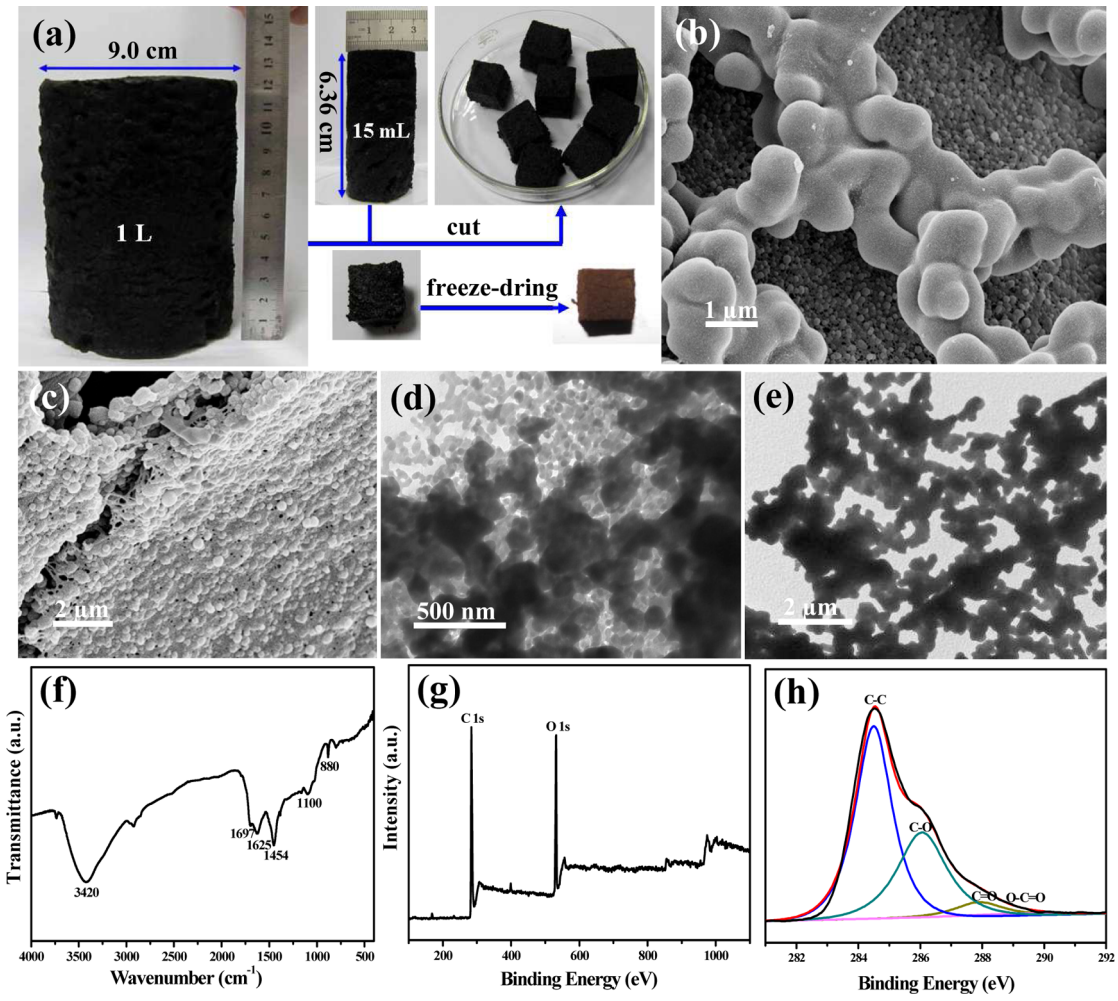

Figure 1. (a) Photographs of the carbonaceous hydrogel monoliths with different volumes and the corresponding carbonaceous aerogel block. SEM images (b,c), TEM images (d,e), FT-IR spectra (f), XPS survey (g), and core-level C 1s (h) of the carbonaceous gels.

green and inexpensive route toward carbonaceous gels. As a sustainable and renewable material, biomass (carbohydrates or crude plants) can be directly transformed into carbon materials by a well-established hydrothermal carbonization (HTC) process under mild heating conditions. HTC carbon materials have shown a variety of potential applications in many fields such as drug delivery, catalysis, energy storage, water purification, gas sensor, and CO_2 sequestration.[18,19] For example, Zhao *et al.* fabricated nitrogen-containing hydrothermal carbons by using D-glucosamine as a biomass precursor, which showed excellent performance for supercapacitors.[20] Herein, a cheap, green, and template-free HTC method has been developed for the first time to fabricate sponge-like carbonaceous hydrogels and aerogels by using watermelon, a common fruit, as the carbon source. Compared with the other methods for hydrogel and aerogel preparation, our synthetic method shows some significant advantages: (1) the carbonaceous gels are prepared by a totally green synthetic method without using any commercial chemicals, which can increase the biocompatibility and broaden their applicability for biomedical applications; (2) one-step synthesis is achieved by using cheap and ubiquitous biomass as the carbon source; and (3) the prepared carbonaceous gels showed extraordinary flexibility as well as high chemical reactivity, which endow them great application potential.

A large number of oxygen-containing functional groups on the surface of carbonaceous gels (CGs) make it easily processable, which leads to easy preparation of the 3D carbonaceous gel-based nanocomposites, that is, decorating the 3D CGs with other nanoparticles. Considering that carbonaceous gels may act as a cheap and soft platform, we synthesized Fe_3O_4/CGs composites by a facile solution approach. The 3D porous structural CGs served as the scaffold, and Fe_3O_4 nanoparticles were evenly embedded into the networks of CGs. After calcination, the Fe_3O_4/CGs composites were transformed to the corresponding magnetite carbon aerogels (MCAs). The MCAs are of good conductivity and keep the porous structure of the original CGs, providing a short movement path for both electrolyte ions and electrons during the electrochemical process.

Thus, the obtained composite materials may have great potential in energy storage.

RESULTS AND DISCUSSION

The sponge-like carbonaceous hydrogel (CG) was prepared by a simple one-pot hydrothermal process directly from the soft tissue biomass of watermelon. The volumes of the CG monolith can be tuned from 10 mL to 1 L by cutting the fresh watermelon into different sized monoliths and using the corresponding volumetric autoclaves. The CG monoliths with the volumes of 15 mL and 1 L are shown in Figure 1a. It can be seen that the black carbonaceous hydrogels have rough surfaces and can be easily cut into smaller sizes. For preparing carbonaceous aerogels, the obtained CG monolith was first cut into smaller sizes by a sharp knife and then freeze-dried to remove the absorbed water. After the freeze-drying process, the color of the carbonaceous hydrogels turned from black to brown (Figure 1a). The mass density of the wet hydrogel and the dry aerogel was measured to be about 1.05 and 0.058 g/m^3, respectively. Thus, the water content in the hydrogel accounts for more than 90% of its weight. In addition, there is no obvious shrinkage observed for the obtained aerogel as compared to the original hydrogel after freeze-drying (Figure 1a). The field emission scanning electron microscopy (FE-SEM) and the transmission electron microscopy (TEM) were applied to look into the microstructure of the CGs. SEM images reveal that the obtained CGs consist of both a global catenulate carbon network and a carbon nanofiber cross-linked carbon nanosphere network that together constitute the 3D porous structure (Figure 1b,c). During the hydrothermal reaction, carbohydrates in the watermelon polymerize and carbonize to form carbonaceous nanospheres and nanofibers while fibrous watermelon tissues are converted to a large catenulate carbon structure. TEM images further show the interconnected networks of the CGs with many irregular ligaments and branches consisting of cross-linked nanospheres and nanoparticles (Figure 1d,e). The pores created by the interconnected networks observed from the TEM images vary from several nanometers to micrometers, and the average pore diameter was measured to be 45.8 nm, which is located in the micropore (<50 nm) region. The presence of a large number of micropores in the CGs allows the efficient diffusion/mass transfer of liquid/gas phase of other components, leading to potential applications as adsorbents as well as substrates.

The surface functional groups of the obtained CGs were identified by Fourier transform infrared (FT-IR) spectroscopy, as shown in Figure 1f. The broad and strong band at 3420 cm^{-1} is attributed to the O−H stretching vibrations. The observed bands at 1697 and 1625 cm^{-1} are attributed to the C═O and C═C stretching vibrations, respectively, indicating the existence of furanic and aromatic groups.[21,22] The bands at about 1454 cm^{-1} can be attributed to either carboxylic O−H deformation vibration or C−H bending vibration.[22] The bands at 1100 and 880 cm^{-1} can be ascribed to the C−O−C stretching vibration and deformation vibration of vinyl C−H, respectively.[23] From the FT-IR analysis, the existence of a large number of functional groups such as hydroxyl, carbonyl, carboxyl, and aromatic groups on the surface of CGs can be deduced. The X-ray photoelectron spectroscopy (XPS) was applied to further verify the aforementioned oxygen-containing groups. The high content of the C and O elements in the CGs was observed by the photoelectron lines at binding energies of about 285 and 711 eV, attributed to C 1s and O 1s, respectively, as displayed in the wide scan XPS spectrum in Figure 1g. The deconvoluted C 1s spectra show the presence of four different carbon groups: graphitic carbon at 284.6 eV (C═C), alcohol, phenolic, and ether groups at 286.5 eV (C−O), the carbonyl carbon at 287.9 eV (C═O), and ester or carboxyl groups at 288.4 eV (C═O−C) (Figure 1h).[24] The XPS analysis also confirms the existence of a large number of oxygen functional groups on the surface of CGs. The presence of oxygen functional groups could be due to the incomplete carbonization of the carbohydrates (*i.e.*, glucose) at a temperature as low as 160−200 °C during the hydrothermal treatment process.[1]

The mechanical properties of the CGs were systematically investigated by the dynamic viscoelastic measurements and the compression tests. As shown in Figure 2a, both the carbonaceous hydrogel and the aerogel can be compressed, and their original dimensions after the release of compression can be easily recovered. The dynamic viscoelastic measurements of the carbonaceous hydrogel (Figure 2b) show that the storage modulus value is much higher than the loss modulus value over the entire angular frequency (1−100 rad·s^{-1}), which reveals that the elastic response is predominant, implying that the carbonaceous hydrogel has a permanent network.[16]

The loss modulus value of the carbonaceous hydrogels slightly changes and does not cross over each other in the entire tested frequency range, indicating a highly cross-linking structure of the gel.[16] These results are consistent with the SEM and TEM observations. The value of the storage modulus at 10 rad·s^{-1} is about 948.5 kPa which is much higher than that of the CNTs hydrogel,[25,26] graphene hydrogel,[16,24] carbonaceous fiber hydrogel,[1] and nanocellular hydrogel.[27] Cyclic stress−strain curves show that both the hydrogel and aerogel can sustain large strain deformations (over 50%). Figure 2c shows the compressive stress−strain curve for the carbonaceous hydrogel at a set strain (ε) of 60% with maximal stress of 23.8 kPa. The curve contains an initial linear region at ε < 30% and then gradually

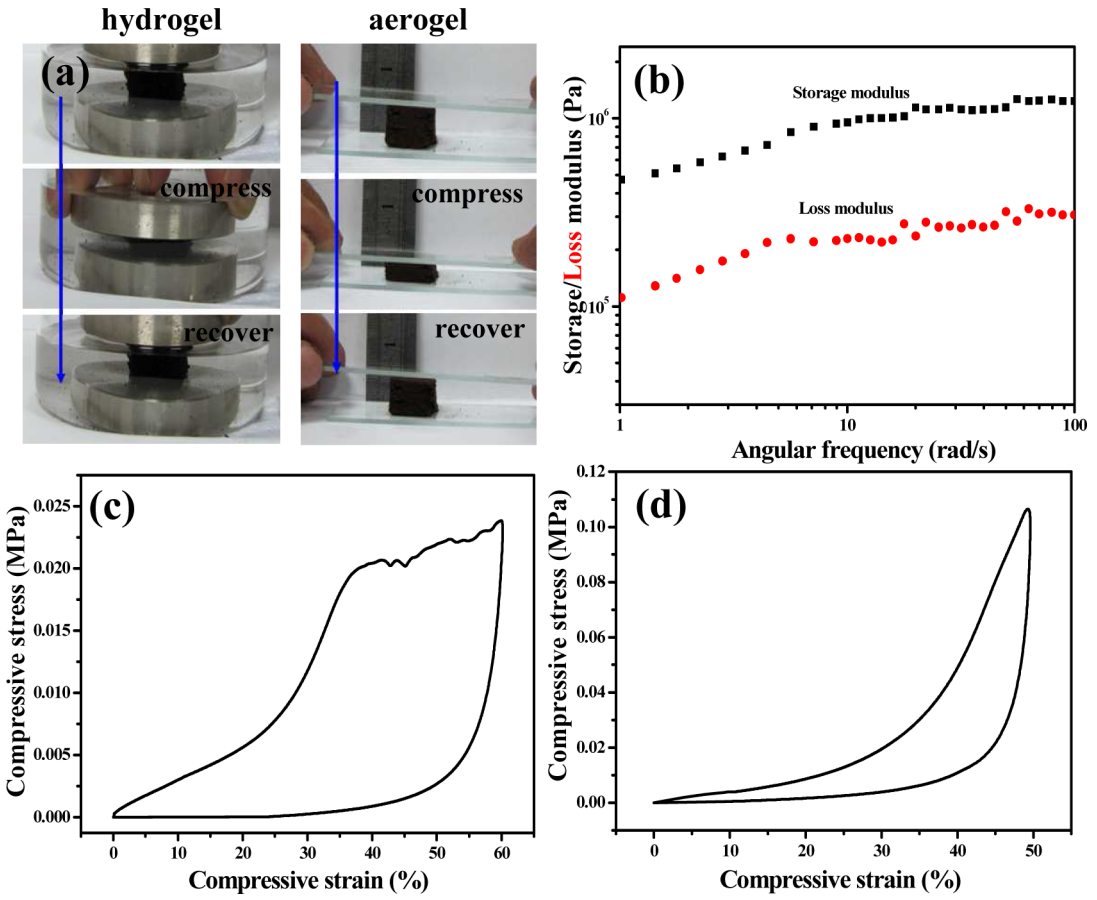

Figure 2. Mechanical properties of the obtained carbonaceous hydrogel and aerogel. (a) Digital photographs illustrating the compressive properties of the hydrogel and aerogel. (b) Dynamic rheological behavior of carbonaceous hydrogel. Compressive stress−strain diagrams of the hydrogel (c) and aerogel (d) at a maximum strain of 60 and 50%, respectively.

increases to a plateau until a strain of up to 60%. The unloading curve also shows that the compressed carbonaceous hydrogel can almost complete recovery of its original volume, as can be clearly seen from the digital pictures in Figure 2a. The compressive stress−strain curve for the carbonaceous aerogel at $\varepsilon = 50\%$ shows higher maximal stress at about 100 kPa (Figure 2d). The strong mechanical properties of both the CGs could be attributed to their unique interconnected 3D network structure, suggesting that the CGs have potential applications as substrates for the synthesis of robust 3D functional composite materials.

Inspired by the idea that the flexible and chemically active CGs can be used as a platform for the synthesis of functional composite materials, we fabricated Fe_3O_4/CG composite materials by a facile one-step solution reaction (see Methods section). After that, the obtained Fe_3O_4/CG composites were transformed into magnetite carbon aerogels (MCAs) by calcination. SEM image (Figure 4a) shows the catenulate carbon network and carbon nanosphere network of the MCAs, indicating that MCAs keep the porous structure of the original CG after the calcination process. TEM image (Figure 4b) further reveals the porous structure of the MCAs and shows the embedded Fe_3O_4 nanoparticles

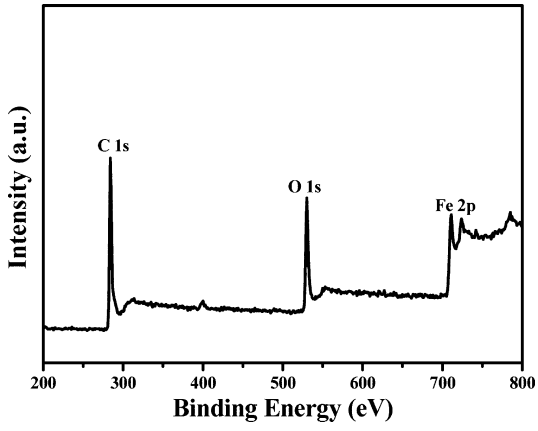

Figure 3. XPS survey of the obtained MCAs, indicating the presence of C, O, and Fe elements.

in the 3D carbon networks. From the magnified TEM image (Figure 4c), it can be observed that the small Fe_3O_4 nanoparticles with average size of about 9 nm were evenly incorporated into the carbon substrate. Figure 4d shows the XRD pattern of the MCA composites. The characterized peaks at about $2\theta = 30.2$, 35.6, 43.2, 53.4, 57.5, and 62.7° can be assigned to the phase of Fe_3O_4 (JCPDS 75-0033).[28] The presence of C, O, and

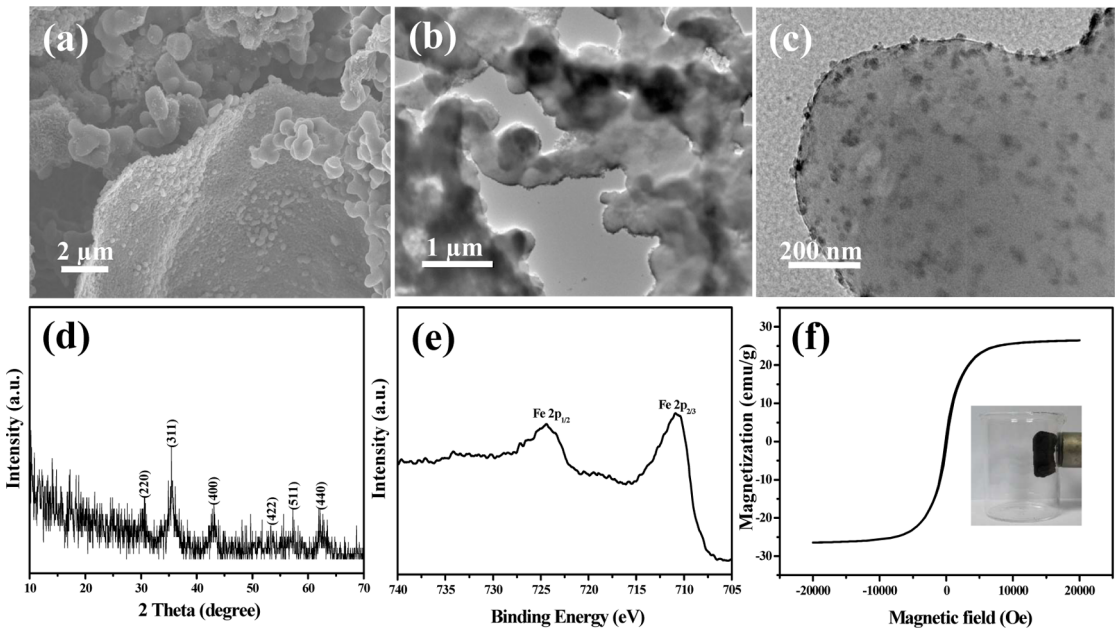

Figure 4. (a) SEM image of the MCA sample. TEM images of the MCAs at low (b) and high (c) magnification. XRD pattern (d), Fe 2p XPS spectrum (e), and room temperature magnetic hysteresis loops (f) of the MCAs. The inset shows the lightweight MCA monolith lifted by a magnet.

Fe elements in the MCA composites was confirmed by the XPS analysis (Figure 3). The Fe 2p spectrum (Figure 4e) shows two characteristic peaks at about 724.4 and 710.9 eV, with a spin energy separation of 13.5 eV, which are attributed to the Fe $2p_{1/2}$ and Fe $2p_{3/2}$ for Fe_3O_4, respectively.[28,29] The room temperature magnetization curve of MCAs was measured in an applied magnetic field from −20 000 to 20 000 Oe (Figure 4f). The specific saturation magnetization (M_s) and magnetic remanence (M_r) of MCAs are 26.6 and 1.4 emu·g^{-1}, respectively. The small M_r value indicates that MCAs exhibit a superparamagnetic behavior. It is advantageous that no magnetization remains when the applied magnetic field is removed. The inset in Figure 4f shows that the lightweight MCA monolith could be lifted by a magnet, which also demonstrated the magnetic properties of the MCA sample.

The obtained MCAs were further applied as electrode materials for supercapacitors. The electrochemical properties of MCAs were investigated by using cyclic voltammogram (CV) and galvanostatic charge/discharge measurements within the potential window of −1.0 to 0 V in 6 M KOH aqueous solution with a three-electrode system. The CV curves measured at potential sweep rates of 5−100 mV·s^{-1} are shown in Figure 5a. The CV curve of the MCAs at a scan rate of 5 mV·s^{-1} has asymmetric shape, which could be due to the contribution of the pseudocapacitance from Fe_3O_4 nanoparticles to the total capacitances.[30] The specific capacitances of MCAs obtained from the CV curves are calculated by the equation $C = (\int I dv)/(\upsilon m V)$, where C is the specific capacitance (F·g^{-1}), I is the current (A), V is the potential window (V), υ is the scan rate (mV·s^{-1}), and m is the mass of the sample used for the electrochemical test (g). The calculated specific capacitances at different scan rate are present in Figure 5b. The MCAs show specific capacitances of 369.2 and 142.3 F·g^{-1} at a scan rate of 5 and 100 mV·s^{-1}, respectively. The obtained specific capacitance at a scan rate of 5 mV·s^{-1} is higher than that of the Fe_3O_4/graphene nanocomposites (341 F·g^{-1}).[31] Charge/discharge behavior of the MCA electrode was also tested at current densities from 0.5 to 10 A·g^{-1}. The charge/discharge curves exhibit almost triangular shape with a small internal resistance (IR) drop at current density of 0.5 A·g^{-1} (Figure 5c), implying a high degree of symmetry in charge and discharge.[32] The presence of the IR drop at the beginning of discharge is usually associated with the equivalent series resistance (ESR) phenomenon.[33] The specific capacitances of MCAs can be calculated from the discharge curves by the equation $C = (I\Delta V)/(m\Delta V)$,[34] where I is the constant discharge current (A), Δt is the discharging time (s), and ΔV is the discharge voltage excluding the IR drop (V). The specific capacitances of MCAs from the discharge curve are calculated to be 337.2 and 333.1 F·g^{-1} at a current density of 0.5 and 1 A·g^{-1}, respectively. The above specific capacitances obtained from the charge/discharge measurements are consistent with those calculated by the CV curves. When discharge current density increases to 6 A·g^{-1}, the MCAs still exhibited considerable capacitances of 222.3 F·g^{-1}. The specific capacitance of MCAs obtained at a current density of 1 A·g^{-1} is comparable to that of Fe_3O_4/graphene nanosheets (358 F·g^{-1}, 6 M KOH electrolyte)[31] and

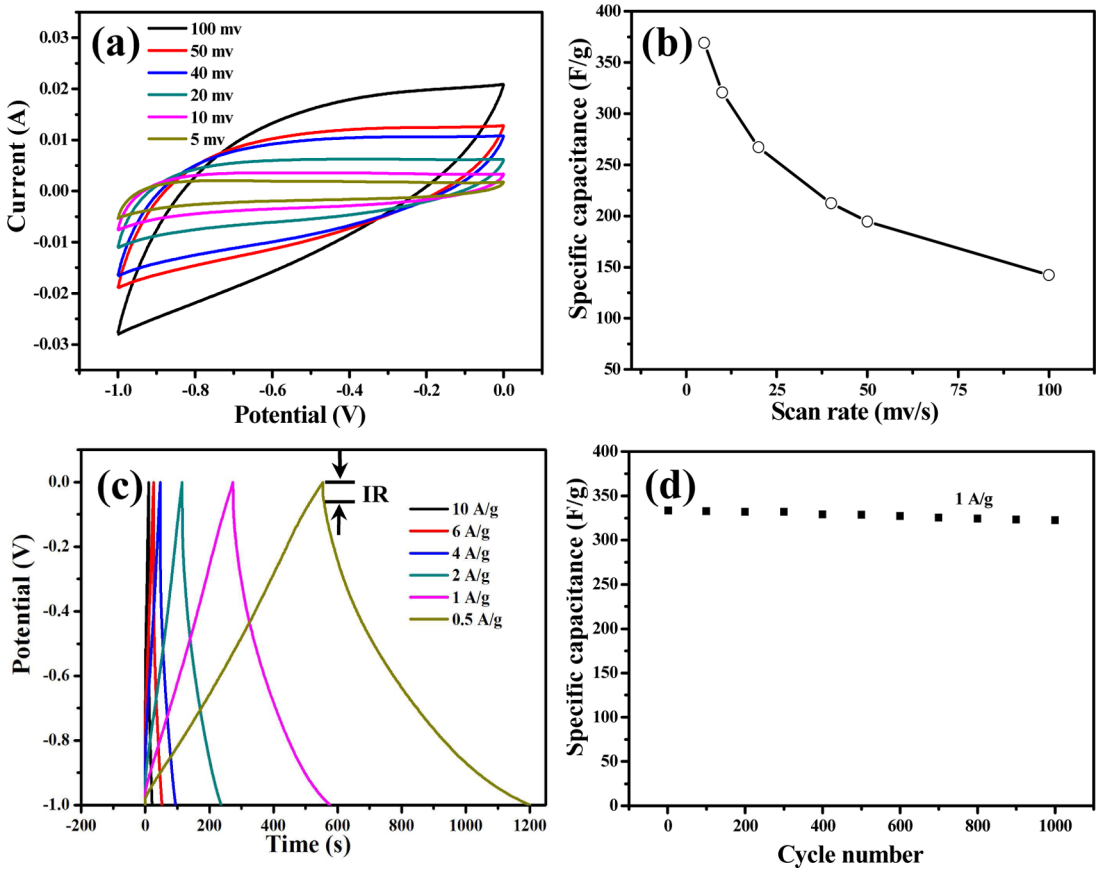

Figure 5. (a) Representative cyclic voltammetry (CV) curves of MCAs electrode. (b) Calculated specific capacitances from the CV curves at different scan rates. (c) Charge/discharge curves of the MCA electrode at different constant current densities. (d) Cycle life of MCA electrode at a charge/discharge current density of 1 A·g^{-1} for 1000 cycles.

MnO_2/chemically modified graphene composites (389 F·g^{-1}, 1 M Na_2SO_4)[35] and much higher than that of many other carbon-based materials such as N-doped carbon fibers (202.0 F·g^{-1}, 6 M KOH electrolyte),[36] Co_3O_4/r-GO composites (163.8 F·g^{-1}, 6 M KOH electrolyte),[37] and N-doped hollow graphitic carbon spheres (260 F·g^{-1}, 2 M H_2SO_4 electrolyte).[38] The high-rate capability also ensures its high energy density, which could be due to the interconnected 3D porous structure of MCAs, providing a short diffusion path for electrolyte ions.[39] The volumetric storage capacity of MCAs was also measured. The value of the volumetric capacitance is about 30.3 F/cm^3, which is much lower than the corresponding gravimetric capacitance. The volumetric capacitance value is lower than that of hierarchical porous carbons (54 F/cm^3)[40] and activated carbon/carbon nanotube composites (47 F/cm^3)[41] but higher than that of carbon nanotubes (<16 F/cm^3).[42,43] This relatively low volumetric performance of MCAs could be attributed to its low mass density due to the presence of a large number of micropores. In order to evaluate the durability of the MCAs, a repetitive charge/discharge test of the electrode at current density of 1 A·g^{-1} over 1000 cycles was carried out. As shown in Figure 5d, the MCAs exhibit the capacitance of 333.1 F·g^{-1} at the first cycle and 322.3 F·g^{-1} at the 1000th cycle; that is, it maintains 96% of the initial capacitance after 1000 charge/discharge cycles. The high durability of the electrode could be ascribed to the robust 3D structure of the MCAs which allow the sustained and stable transport of both electrolyte ions and electrons to the electrode surface. The inexpensive raw materials used, the high capacitance, and good cycling stability offer MCAs as promising electrode materials for supercapacitors.

To further investigate the behavior of the MCA electrode for supercapacitors, the electrochemical impedance spectroscopy (EIS) analysis was carried out in a frequency range from 0.01 Hz to 0.1 MHz. The Nyquist plot of the MCA is shown in Figure 6. The inset shows the equivalent circuit for the fitting of the EIS data, where R_s is the solution resistance, C_{dl} is a double-layer capacitor, R_{ct} is the charge transfer resistance, W is the Warburg impedance, and C_L is the limit pseudocapacitor.[32] It can be observed that the Nyquist plot has two distinct parts, a semicircle part at high frequency and a linear part at low frequency. At high frequency, the solution resistance and the charge transfer resistance can be obtained from the intercept at real axis (Z') and the semicircle intercepts in the Nyquist plot, respectively.[34] The R_s and R_{ct} for the MCA

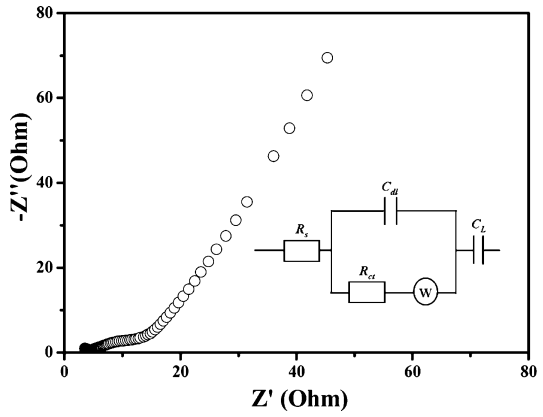

Figure 6. Nyquist curves and inset showing the electrical equivalent circuit used for fitting the impedance spectra.

electrode were measured to be 4.4 and 8.7 Ω, respectively. In the middle frequency, the inclined portion of the curve (about 45°) is ascribed to the Warburg impedance, which is responsible for the frequency dependence of ion diffusion/transport from the electrolyte to the electrode surface.[44] The magnitude of ESR obtained from the intercept of the Nyquist plot is about 12.2 Ω, which is responsible for the IR drop at the beginning of discharge, in accordance with the results of the charge−discharge experiment.[33]

SUMMARY AND CONCLUSIONS

We have developed a simple and efficient method for preparing low-cost carbonaceous flexible hydrogels and aerogels by using crude biomass watermelon as the carbon source. The carbonaceous gels have a 3D porous structure and exhibit high chemical activity and robust mechanical properties, providing tremendous potential as scaffold for synthesizing 3D composite materials. We further fabricated the carbonaceous gel-based composite materials by embedding Fe_3O_4 nanoparticles into the networks of the carbonaceous gels. The results show that the MCA composite material is beneficial for the transportation of both electrolyte ions and electrons, leading to high electrochemical performance. The MCAs exhibit excellent capacitance of 333.1 $F \cdot g^{-1}$ at a current density of 1 $A \cdot g^{-1}$ and outstanding cycling stability with 96% of the capacitance retention after 1000 charge/discharge cycles. Our results demonstrate that the obtained elastic carbonaceous gels can be a predominant substrate to synthesize other 3D composite materials with excellent integrated properties. Furthermore, benefiting from the 3D porous structure, the low cost of the precursors, and the green route, the obtained flexible carbonaceous gels offer very attractive prospects and could be extended to the applications as adsorbents, supporter for sensors, and biomedical materials.

METHODS

Synthesis of Carbonaceous Gels and Magnetite Carbon Aerogels. The carbonaceous hydrogel was prepared by a simple one-pot hydrothermal reaction. Watermelon was first cut into the appropriate volume and then put into a Teflon-lined stainless-steel autoclave. After that, the autoclave was put into an oven and heated at 180 °C for 12 h. Black carbonaceous hydrogel monolith was obtained after the hydrothermal reactions. The product was immersed in water and ethanol for several days to remove the soluble impurities. The corresponding carbonaceous aerogel was obtained by cutting the carbonaceous hydrogel monolith into small pieces followed by freeze-drying. To prepare the MCAs, a piece of carbonaceous aerogel with a dimension of about 2 × 3 × 3 cm^3 was fully immersed in a 20 mL aqueous solution containing 1.30 g of $FeCl_3$ (8 mmol) and $FeSO_4 \cdot 7H_2O$ (1.25 g, 4.5 mmol) for 15 min under N_2 protection. The mixture was heated to 80 °C, and a large amount of N_2 was introduced into liquid to stir the liquid. After that, 10 mL of 30% ammonia solution was added to the mixture and kept at 80 °C for 30 min. At last, 3.0 g of trisodium citrate was added to the solution while the temperature increased to 95 °C. The obtain Fe_3O_4/carbonaceous, hydrogel composites were rinsed by Milli-Q water and dried in an oven at 70 °C. To obtain the MCAs, the above Fe_3O_4/carbonaceous hydrogel composites were calcined in N_2 atmosphere at 550 °C for 4 h.

Characterization. Field emission scanning electron microscopy (FE-SEM) (JEOL JSM-6330F) and transmission electron microscopy (TEM) (JEOL-2010) were applied to look into the microstructure of the carbonaceous gels and MCAs. The surface states of the carbonaceous gels and MCAs were characterized by X-ray photoelectron spectroscopy (XPS) (VG Scientific ESCALAB Mark II spectrometer). Fourier transform infrared (FT-IR) spectra (Nicolet Magana-IR 750 spectrometer) were used to determine the surface functional groups of the carbonaceous gels. The X-ray diffraction (XRD) pattern of the sample was recorded on a Philips X'Pert Pro Super X-ray diffractometer (Cu Kα source, λ = 1.54178 Å). The magnetic property of the MCAs was investigated by a magnetometer (Quantum Design MPMS XL) at 300 K with an applied magnetic field of 20 kOe. The mechanical properties of the carbonaceous gels were investigated by the dynamic viscoelastic measurements and the compression tests on an dynamic mechanical analyzer (DMA Q800, TA Instruments, USA) using a double cantilever measuring mode.

Electrochemical Measurements. All electrochemical experiments were carried out on a CHI660a electrochemical workstation (Shanghai Chenhua Instruments Co.) at room temperature. The working electrode was prepared by loading a slurry containing 80 wt % MCA (about 2 mg), 10 wt % poly(vinylidene fluoride) (PVDF) (in *N*-methylpyrrolidone), and 10 wt % acetylene black on a nickel foam. After the electrode materials were loaded, the working electrode was pressed and dried in vacuum at 80 °C for 12 h. In a three-electrode system, the above loaded nickel foam as working electrode was investigated with a Pt counter electrode and Ag/AgCl reference electrode in 6 M KOH solution as the electrolyte. CV curves were obtained in the potential range of −1.0 to 0 V *vs* Ag/AgCl by varying the scan rate from 5 to 100 $mV \cdot s^{-1}$. Charge/discharge measurements were carried out with a constant current at 0.5−10.0 $A \cdot g^{-1}$ with a potential window of −1.0 to 0 V. Electrochemical impedance spectroscopy (EIS) measurements were conducted for the working electrode in a frequency range of 100 kHz to 0.01 Hz with ac perturbation of 5 mV. The EIS data were analyzed using Nyquist plots, which represent the imaginary part (Z') and real part (Z'') of impedance.

Conflict of Interest: The authors declare no competing financial interest.

Acknowledgment. We acknowledge financial support by the National Basic Research Program of China (2010CB934700, 2011CB933700), National Natural Science Foundation of China (21271165, 21225730), and Hefei Center for physical science and technology (2012FXZY005).

REFERENCES AND NOTES

1. Liang, H. W.; Guan, Q. F.; Chen, L. F.; Zhu, Z.; Zhang, W. J.; Yu, S. H. Macroscopic-Scale Template Synthesis of Robust Carbonaceous Nanofiber Hydrogels and Aerogels and Their Applications. *Angew. Chem., Int. Ed.* **2012**, *51*, 5101–5105.
2. White, R. J.; Budarin, V.; Luque, R.; Clark, J. H.; Macquarrie, D. J. Tuneable Porous Carbonaceous Materials from Renewable Resources. *Chem. Soc. Rev.* **2009**, *38*, 3401–3418.
3. Xue, Z.; Wang, S.; Lin, L.; Chen, L.; Liu, M.; Feng, L.; Jiang, L. A Novel Superhydrophilic and Underwater Superoleophobic Hydrogel-Coated Mesh for Oil/Water Separation. *Adv. Mater.* **2011**, *23*, 4270–4273.
4. Seliktar, D. Designing Cell-Compatible Hydrogels for Biomedical Applications. *Science* **2012**, *336*, 1124–1128.
5. Hendrickson, G. R.; Lyon, L. A. Bioresponsive Hydrogels for Sensing Applications. *Soft Matter* **2009**, *5*, 29–35.
6. Li, J.; Liu, C. Y.; Liu, Y. Au/Graphene Hydrogel: Synthesis, Characterization and Its Use for Catalytic Reduction of 4-Nitrophenol. *J. Mater. Chem.* **2012**, *22*, 8426–8430.
7. Chen, J.; Sheng, K.; Luo, P.; Li, C.; Shi, G. Graphene Hydrogels Deposited in Nickel Foams for High-Rate Electrochemical Capacitors. *Adv. Mater.* **2012**, *24*, 4569–4573.
8. Rolison, D. R.; Long, J. W.; Lytle, J. C.; Fischer, A. E.; Rhodes, C. P.; McEvoy, T. M.; Bourg, M. E.; Lubers, A. M. Multifunctional 3D Nanoarchitectures for Energy Storage and Conversion. *Chem. Soc. Rev.* **2009**, *38*, 226–252.
9. Chien, H. C.; Cheng, W. Y.; Wang, Y. H.; Lu, S. Y. Ultrahigh Specific Capacitances for Supercapacitors Achieved by Nickel Cobaltite/Carbon Aerogel Composites. *Adv. Funct. Mater.* **2012**, *22*, 5038–5043.
10. Wang, J.; Chen, M.; Wang, C.; Wang, J.; Zheng, J. A Facile Method To Prepare Carbon Aerogels from Amphiphilic Carbon Material. *Mater. Lett.* **2012**, *68*, 446–449.
11. Fellinger, T. P.; White, R. J.; Titirici, M. M.; Antonietti, M. Borax-Mediated Formation of Carbon Aerogels from Glucose. *Adv. Funct. Mater.* **2012**, *22*, 3254–3260.
12. Lu, Y.; Sun, Q.; Yang, D.; She, X.; Yao, X.; Zhu, G.; Liu, Y.; Zhao, H.; Li, J. Fabrication of Mesoporous Lignocellulose Aerogels from Wood *via* Cyclic Liquid Nitrogen Freezing−Thawing in Ionic Liquid Solution. *J. Mater. Chem.* **2012**, *22*, 13548–13557.
13. Korhonen, J. T.; Hiekkataipale, P.; Malm, J.; Karppinen, M.; Ikkala, O.; Ras, R. H. A. Inorganic Hollow Nanotube Aerogels by Atomic Layer Deposition onto Native Nanocellulose Templates. *ACS Nano* **2011**, *5*, 1967–1974.
14. Cheng, E.; Li, Y.; Yang, Z.; Deng, Z.; Liu, D. DNA-SWNT Hybrid Hydrogel. *Chem. Commun.* **2011**, *47*, 5545–5547.
15. Zou, J.; Liu, J.; Karakoti, A. S.; Kumar, A.; Joung, D.; Li, Q.; Khondaker, S. I.; Seal, S.; Zhai, L. Ultralight Multiwalled Carbon Nanotube Aerogel. *ACS Nano* **2010**, *4*, 7293–7302.
16. Xu, Y.; Sheng, K.; Li, C.; Shi, G. Self-Assembled Graphene Hydrogel *via* a One-Step Hydrothermal Process. *ACS Nano* **2010**, *4*, 4324–4330.
17. Xu, Z.; Zhang, Y.; Li, P.; Gao, C. Strong, Conductive, Lightweight, Neat Graphene Aerogel Fibers with Aligned Pores. *ACS Nano* **2012**, *6*, 7103–7113.
18. Hu, B.; Wang, K.; Wu, Li.; Yu, S. H.; Antonietti, M.; Titirici, M. M. Engineering Carbon Materials from the Hydrothermal Carbonization Process of Biomass. *Adv. Mater.* **2010**, *22*, 813–828.
19. Titirici, M. M.; Antonietti, M. Chemistry and Materials Options of Sustainable Carbon Materials Made by Hydrothermal Carbonization. *Chem. Soc. Rev.* **2010**, *39*, 103–116.
20. Zhao, L.; Fan, L. Z.; Zhou, M. Q.; Guan, H.; Qiao, S.; Antonietti, M.; Titirici, M. M. Nitrogen-Containing Hydrothermal Carbons with Superior Performance in Supercapacitors. *Adv. Mater.* **2010**, *22*, 5202–5206.
21. Sun, X.; Li, Y. Colloidal Carbon Spheres and Their Core/Shell Structures with Noble-Metal Nanoparticles. *Angew. Chem., Int. Ed.* **2004**, *43*, 597–601.
22. Moreno-Castilla, C.; López-Ramón, M. V.; Carrasco-Marín, F. Changes in Surface Chemistry of Activated Carbons by Wet Oxidation. *Carbon* **2000**, *38*, 1995–2001.
23. Grzyb, B.; Hildenbrand, C.; Berthon-Fabry, S.; Bégin, D.; Job, N.; Rigacci, A.; Achard, P. Functionalisation and Chemical Characterization of Cellulose-Derived Carbon Aerogels. *Carbon* **2010**, *48*, 2297–2307.
24. Cong, H. P.; Ren, X. C.; Wang, P.; Yu, S. H. Macroscopic Multifunctional Graphene-Based Hydrogels and Aerogels by a Metal Ion Induced Self-Assembly Process. *ACS Nano* **2012**, *6*, 2693–2703.
25. Kar, T.; Manda, S. K.; Das, P. K. Influence of Pristine SWNTs in Supramolecular Hydrogelation: Scaffold for Superior Peroxidase Activity of Cytochrome *c*. *Chem. Commun.* **2012**, *48*, 8389–8391.
26. Fukushima, T.; Kosaka, A.; Ishimura, Y.; Yamamoto, T.; Takigawa, T.; Ishii, N.; Aida, T. Molecular Ordering of Organic Molten Salts Triggered by Single-Walled Carbon Nanotubes. *Science* **2003**, *300*, 2072–2074.
27. Pääkkö, M.; Ankerfors, M.; Kosonen, H.; Nykänen, A.; Ahola, S.; Österberg, M.; Ruokolainen, J.; Laine, J.; Larsson, P. T.; Ikkala, O.; *et al.* Enzymatic Hydrolysis Combined with Mechanical Shearing and High-Pressure Homogenization for Nanoscale Cellulose Fibrils and Strong Gels. *Biomacromolecules* **2007**, *8*, 1934–1947.
28. Wu, X. L.; Wang, L.; Chen, C. L.; Xu, A. W.; Wang, X. K. Water-Dispersible Magnetite-Graphene-LDH Composites for Efficient Arsenate Removal. *J. Mater. Chem.* **2011**, *21*, 17353–17359.
29. Chen, W.; Li, S.; Chen, C.; Yan, L. Self-Assembly and Embedding of Nanoparticles by *In Situ* Reduced Graphene for Preparation of a 3D Graphene/Nanoparticle Aerogel. *Adv. Mater.* **2011**, *23*, 5679–5683.
30. Mu, J.; Chen, B.; Guo, Z.; Zhang, M.; Zhang, Z.; Zhang, P.; Shao, C.; Liu, Y. Highly Dispersed Fe_3O_4 Nanosheets on One-Dimensional Carbon Nanofibers: Synthesis, Formation Mechanism, and Electrochemical Performance as Supercapacitor Electrode Materials. *Nanoscale* **2011**, *3*, 5034–5040.
31. Zhang, W.; Liu, F.; Li, Q.; Shou, Q.; Cheng, J.; Zhang, L.; Nelson, B. J.; Zhang, X. Transition Metal Oxide and Graphene Nanocomposites for High-Performance Electrochemical Capacitors. *Phys. Chem. Chem. Phys.* **2012**, *14*, 16331–16337.
32. Yang, S.; Wu, X. L.; Chen, C.; Dong, H.; Hu, W.; Wang, X. Spherical α-$Ni(OH)_2$ Nanoarchitecture Grown on Graphene as Advanced Electrochemical Pseudocapacitor Materials. *Chem. Commun.* **2012**, *48*, 2773–2775.
33. Wang, H.; Liu, Z.; Chen, X.; Han, P.; Dong, S.; Cui, G. Exfoliated Graphite Nanosheets/Carbon Nanotubes Hybrid Materials for Superior Performance Supercapacitors. *J. Solid State Electrochem.* **2011**, *15*, 1179–1184.
34. Lei, Z.; Shi, F.; Lu, L. Incorporation of MnO_2-Coated Carbon Nanotubes between Graphene Sheets as Supercapacitor Electrode. *ACS Appl. Mater. Interfaces* **2012**, *4*, 1058–1064.
35. Choi, B. G.; Yang, M. H.; Hong, W. H.; Choi, J. W.; Huh, Y. S. 3D Macroporous Graphene Frameworks for Supercapacitors with High Energy and Power Densities. *ACS Nano* **2012**, *6*, 4020–4028.
36. Chen, L. F.; Zhang, X. D.; Liang, H. W.; Kong, M.; Guan, Q. F.; Chen, P.; Wu, Z. Y.; Yu, S. H. Synthesis of Nitrogen-Doped Porous Carbon Nanofibers as an Efficient Electrode Material for Supercapacitors. *ACS Nano* **2012**, *6*, 7092–7102.
37. Zhou, W.; Liu, J.; Chen, T.; Tan, K. S.; Jia, X.; Luo, Z.; Cong, C.; Yang, H.; Li, C. M.; Yu, T. Fabrication of Co_3O_4-Reduced Graphene Oxide Scrolls for High-Performance Supercapacitor Electrodes. *Phys. Chem. Chem. Phys.* **2011**, *13*, 14462–14465.

38. Ma, F.; Zhao, H.; Sun, L.; Li, Q.; Huo, L.; Xia, T.; Gao, S.; Pang, G.; Shi, Z.; Feng, S. A Facile Route for Nitrogen-Doped Hollow Graphitic Carbon Spheres with Superior Performance in Supercapacitors. *J. Mater. Chem.* **2012**, *22*, 13464–13468.
39. Zhu, H.; Wang, X.; Liu, X.; Yang, X. Integrated Synthesis of Poly(*o*-phenylenediamine)-Derived Carbon Materials for High Performance Supercapacitors. *Adv. Mater.* **2012**, *24*, 6524–6529.
40. Xia, K.; Gao, Q.; Jiang, J.; Hu, J. Hierarchical Porous Carbons with Controlled Micropores and Mesopores for Supercapacitor Electrode Materials. *Carbon* **2008**, *46*, 1718–1726.
41. Taberna, P. N.; Chevallier, G.; Simon, P.; Pleée, D.; Aubert, T. Activated Carbon−Carbon Nanotube Composite Porous Film for Supercapacitor Applications. *Mater. Res. Bull.* **2006**, *41*, 478–484.
42. Futaba, D. N.; Hata, K.; Yamada, T.; Hiraoka, T.; Hayamizu, Y.; Kakudate, Y.; Tanaike, O.; Hatori, H.; Yumura, M.; Iijima, S. Shape-Engineerable and Highly Densely Packed Single-Walled Carbon Nanotubes and Their Application as Supercapacitor Electrodes. *Nat. Mater.* **2006**, *5*, 987–994.
43. Emmenegger, C.; Mauron, P.; Sudan, P.; Wenger, P.; Hermann, V.; Gallay, R.; Züttel, A. Investigation of Electrochemical Double-Layer (ECDL) Capacitors Electrodes Based on Carbon Nanotubes and Activated Carbon Materials. *J. Power Sources* **2003**, *124*, 321–329.
44. Shi, W.; Zhu, J.; Sim, D. H.; Tay, Y. Y.; Lu, Z.; Zhang, X.; Sharma, Y.; Srinivasan, M.; Zhang, H.; Hng, H. H.; *et al.* Achieving High Specific Charge Capacitances in Fe_3O_4/Reduced Graphene Oxide Nanocomposites. *J. Mater. Chem.* **2011**, *21*, 3422–3427.